

Supporting Information

10 × faster synthesis of chalcogenide solid solutions with tunable S:Se ratio by NaBH₄-activated S+Se precursors

1. Experiment Details

1.1 Chemicals

Copper chloride dihydrate (CuCl₂·2H₂O, ≥ 99.0%), zinc sulfate heptahydrate (ZnSO₄·7H₂O, ≥ 99.5%), stannous mono-sulphate (SnSO₄, ≥ 99.0%), and indium chloride (InCl₃, ≥ 99.5%), selenium (Se, ≥ 99.9%), Sulfur (S, ≥ 99.9%), sodium borohydride (NaBH₄, ≥ 97.0%), polyvinyl pyrrolidone (PVP, K30), ethylenediamine (en, ≥ 99.0%) were purchased and used as received.

1.2 Synthesis of Cu₂ZnSn(S_{1-x}Se_x)₄ solid solution

Cu₂ZnSn(S_{1-x}Se_x)₄ nanocrystals with different x values were prepared using this two-step solvothermal method. In step (i), five samples were prepared by mixing S powder and Se powder with different molar ratios of S:Se (3:1, 2:1, 1:1, 1:2, 1:3, respectively) as chalcogen sources. Then, 2 mmol NaBH₄, 2 mmol chalcogen source and 10 ml en were added into a 25 ml autoclave. The autoclave was sealed and maintained at 200 °C for 2 h to prepare liquid activated chalcogen precursors. In step (ii), 1 mmol CuCl₂·2H₂O, 0.5 mmol ZnSO₄·7H₂O and 0.5 mmol SnSO₄ were used to prepare the metal precursor by dissolving these metal salts in 10 ml deionized water together with 0.9 g PVP with magnetic stirring. The resulting mixture was loaded into the autoclave which contained the activated chalcogen precursor prepared in step (i) and a solvothermal reaction occurred at 200 °C for 2 h.

1.3 Synthesis of CuIn(S_{1-x}Se_x)₂ solid solution

CuIn(S_{1-x}Se_x)₂ nanocrystals with different x values were prepared by using this two-step solvothermal method. In step (i), five samples were prepared by mixing S powder and Se powder with different molar ratios of S:Se (3:1, 2:1, 1:1, 1:2, 1:3, respectively) as chalcogen sources. Then, 2 mmol NaBH₄, 2 mmol chalcogen source and 10 ml en were added into a 25 ml autoclave. The autoclave was sealed and maintained at 200 °C for 2 h to prepare liquid activated chalcogen precursors. In step (ii), 1 mmol CuCl₂·2H₂O, 1 mmol InCl₃ were used to prepare the metal precursor by dissolving these metal salts in 10 ml deionized water together with 0.9 g PVP with magnetic stirring. The resulting mixture was loaded into the autoclave which contained the activated chalcogen precursor prepared in step (i) and a solvothermal reaction occurred at 200 °C for 2 h.

1.4 Synthesis of Cu_{2-y}(S_{1-x}Se_x) solid solution

Cu_{2-y}(S_{1-x}Se_x) nanocrystals with different x values were prepared by using this two-step solvothermal method. In step (i), five samples were prepared by mixing S powder and Se powder with different molar ratios of S:Se (3:1, 2:1, 1:1, 1:2, 1:3, respectively) as chalcogen sources. Then, 2 mmol NaBH₄, 2 mmol chalcogen source and 10 ml en were added into a 25 ml autoclave. The autoclave was sealed and maintained at 200 °C for 2 h to prepare liquid activated chalcogen precursors. In step (ii), 4 mmol CuCl₂·2H₂O were used to prepare the metal precursor by dissolving these metal salts in 10 ml deionized water together with 0.9 g PVP with magnetic stirring. The resulting mixture was loaded into the autoclave which contained the activated chalcogen precursor prepared in step (i) and a solvothermal reaction occurred at 200 °C for 2 h.

After the autoclave was cooled to room temperature naturally, black precipitates were collected and washed with deionized water or ethanol for 5 times. The synthesized nanoparticles were dispersed in deionized water

ultimately.

1.5 Characterizations

The SEM images and EDS data are taken using a ZEISS EVO@ LS15 SEM equipped with a Bruker Nano GmbH XFlash Detector 5010. XRD data was identified by using a Bruker D8 ADVANCE with Cu-K α ($k = 1.5418 \text{ \AA}$) radiation source and collected with an angle increment of 0.02° at a scan rate of 0.1 s/step . Raman spectra of $\text{Cu}_2\text{ZnSn}(\text{S}_{1-x}\text{Se}_x)_4$ solid solution were obtained using a Raman spectroscopy (Renishaw inVia). UV-Vis spectra were characterized by using a UV-VIS-NIR spectrophotometer (Agilent, Cary 5000). High-resolution transmission electron microscopy (HRTEM) images were taken with a Tecnai G2 F30 TEM at an accelerating voltage of 300 kV. A sample of $\text{Cu}_2\text{ZnSn}(\text{S}_{1-x}\text{Se}_x)_4$ solid solution for TEM analysis was prepared by placing a drop of the its anhydrous alcohol solution on a carbon-coated copper grid and letting it dry in air.

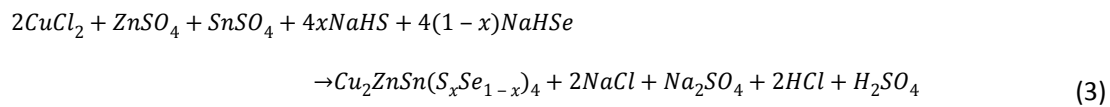
2. Possible reactions involved in the formation of $\text{Cu}_2\text{ZnSn}(\text{S}_{1-x}\text{Se}_x)_4$

The possible chemical reactions involved in the presented two-step synthesis of $\text{Cu}_2\text{ZnSn}(\text{S}_{1-x}\text{Se}_x)_4$ are described as follows:

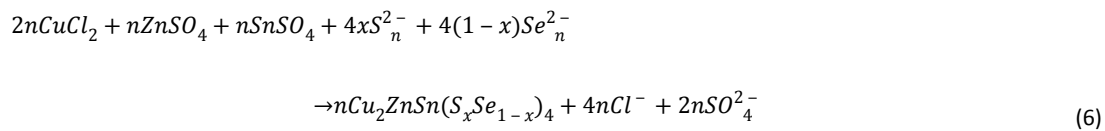
Step (i)



Step (ii)



Additionally, the following reaction also is possible in step (ii) because aqueous solution of metal salts introduces H_2O into the reaction system:



3. Supplemental data about $\text{Cu}_2\text{ZnSn}(\text{S}_{1-x}\text{Se}_x)_4$ solid solution

Table S1 Comparisons of the necessary reaction time of solvothermal synthesis of chalcogenides

Ref No.	Solvent	Raw materials	Temperature	Reaction time	Product
This work	ethylenediamine	$\text{CuCl}_2 \cdot 2\text{H}_2\text{O}$, $\text{ZnSO}_4 \cdot 7\text{H}_2\text{O}$, SnSO_4 , NaBH_4 activated Chalcogen precursor, and PVP	200°C	2 h	$\text{Cu}_2\text{ZnSn}(\text{S}_{1-x}\text{Se}_x)_4$ ($0 < x < 1$)
13	ethylenediamine	CuCl , ZnCl_2 , $\text{SnCl}_4 \cdot 5\text{H}_2\text{O}$, Se and S powder	200°C	24 h	$\text{Cu}_2\text{ZnSnS}_x\text{Se}_{4-x}$ ($0 \leq x \leq 4$)
14	ethylenediamine	$\text{CuCl}_2 \cdot 2\text{H}_2\text{O}$, InCl_3 , GaCl_3 , Se	250°C	24 h	$\text{Cu}(\text{In}_{1-x}\text{Ga}_x)\text{Se}_2$
15	ethylene glycol, triethanolamine	$\text{Zn}(\text{NO}_3)_2 \cdot 6\text{H}_2\text{O}$, NaOH , Se powder	180°C	24 h	ZnSe
16	ethylene glycol	$\text{CuCl}_2 \cdot 2\text{H}_2\text{O}$, ZnCl_2 , $\text{SnCl}_4 \cdot 5\text{H}_2\text{O}$, Se, PVP	250°C	24 h	$\text{Cu}_2\text{ZnSnSe}_4$
17	oleylamine	CuCl , ZnCl_2 , $\text{SnCl}_4 \cdot 5\text{H}_2\text{O}$, Se	250°C	72 h	$\text{Cu}_2\text{ZnSnSe}_4$

18	ethylenediamine	CuCl, SnCl ₄ ·5H ₂ O, Cd(NO ₃) ₂ ·4H ₂ O, Zn(CH ₃ COO) ₂ ·2H ₂ O, Se powder, N ₂ H ₄ ·H ₂ O	190 °C	24 h	Cu ₂ ZnSnSe ₄ or Cu ₂ CdSnSe ₄
19	ethylenediamine	CuCl ₂ ·2H ₂ O, InCl ₃ ·4H ₂ O, Se	180 °C	18 h	CuInSe ₂

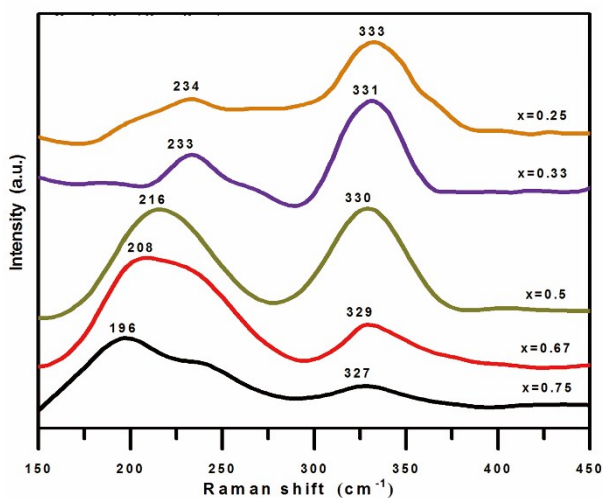


Fig. S1 Raman Spectra of Cu₂ZnSn(S_{1-x}Se_x)₄ NCs samples with different x values that synthesized with the activated chalcogen precursor at 200 °C for 2 h.

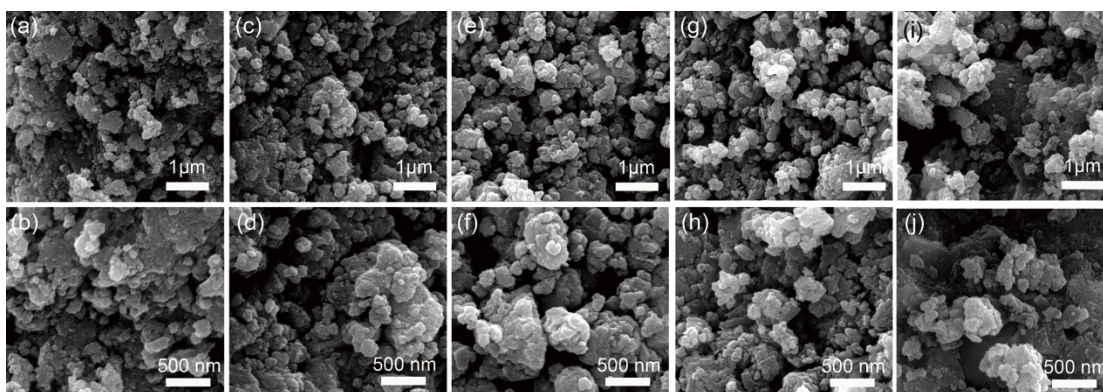


Fig S2 SEM images of Cu₂ZnSn(S_{1-x}Se_x)₄ NCs samples with different x values that synthesized with the activated chalcogen precursor at 200 °C for 2 h: (a), (b) x=0.25; (c), (d) x=0.33; (e), (f) x=0.5; (g), (h) x=0.67; (i), (j) x=0.75

Table S2 Yield of the presented time-saving solvothermal synthesis of chalcogenide solid solutions

Sample No.	Target product	Mass of starting materials (g)					Mass of products (g)		Yield (%)	Avg. yield (%)
		CuCl ₂ ·2H ₂ O	ZnSO ₄ ·7H ₂ O	SnSO ₄	S	Se	Theoretical*	experimental		
1	Cu ₂ ZnSn(S _{0.75} Se _{0.25}) ₄	0.1709	0.1433	0.1075	0.0484	0.0398	0.2432	0.2106	86.60	86.25
		0.1704	0.1438	0.1074	0.0480	0.0395		0.2091	85.98	
		0.1705	0.1440	0.1078	0.0486	0.0393		0.2096	86.18	
2	Cu ₂ ZnSn(S _{0.67} Se _{0.33}) ₄	0.1707	0.1444	0.1076	0.0430	0.0524	0.2504	0.2061	82.31	82.80
		0.1705	0.1442	0.1078	0.0427	0.0521		0.2086	83.31	
		0.1703	0.1439	0.1074	0.0425	0.0526		0.2073	82.79	
3	Cu ₂ ZnSn(S _{0.5} Se _{0.5}) ₄	0.1710	0.1438	0.1079	0.0320	0.0789	0.2666	0.2263	84.88	84.63
		0.1707	0.1435	0.1074	0.0321	0.0792		0.2249	84.36	
		0.1709	0.1441	0.1077	0.0325	0.0790		0.2257	84.66	
4	Cu ₂ ZnSn(S _{0.33} Se _{0.67}) ₄	0.1707	0.1440	0.1074	0.0216	0.1049	0.2818	0.2395	84.99	83.43
		0.1708	0.1439	0.1073	0.0215	0.1053		0.2339	83.00	
		0.1705	0.1443	0.1076	0.0211	0.1050		0.2318g	82.30	
5	Cu ₂ ZnSn(S _{0.25} Se _{0.75}) ₄	0.1704	0.1441	0.1073	0.0163	0.1185	0.2901	0.2524	87.00	87.13

0.1705	0.1437	0.1078	0.0160	0.1182	0.2541	87.59
0.1709	0.1438	0.1074	0.0165	0.1187	0.2518	86.80

*Calculated based on the mole of the starting materials

4. Characterization of as-synthesized $\text{Cu}_2\text{ZnSnSe}_4$

Fig. S3 shows an XRD pattern and a Raman spectrum of $\text{Cu}_2\text{ZnSnSe}_4$ (CZTSe) prepared at 200 °C with the NaBH_4 -activated chalcogen precursors in 2 h. The diffraction peaks in Fig. S3 (a), which are well indexed to planes (112), (204), and (312) respectively, can be assigned to kesterite $\text{Cu}_2\text{ZnSnSe}_4$ (JCPDS No. 52-0868) and no split peaks are found. Phase composition of CZTSe sample was further confirmed by Raman spectroscopy. Three Raman peaks in Fig S3 (b) located at 158, 190, and 225 cm^{-1} are observed, which are in close agreement with that reported in Ref 32-34. The Composition of the as-synthesized CZTSe is close to the stoichiometric chemical compositions (determined by EDS).

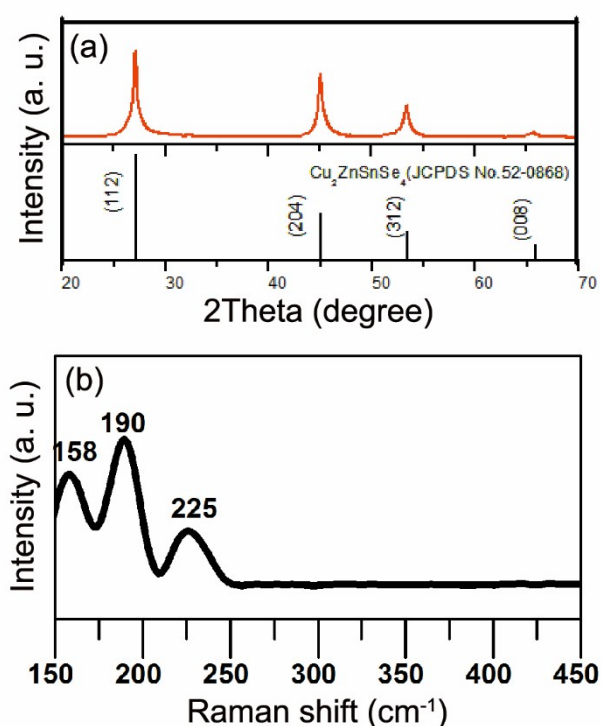


Fig. S3 XRD pattern (a) and Raman Spectrum (b) of solvothermal synthesized $\text{Cu}_2\text{ZnSn}(\text{S}_{0.5}\text{Se}_{0.5})_4$ nanocrystals prepared by NaBH_4 -activated chalcogen precursors.

5. Characterization of as-synthesized $\text{Cu}_{2-y}(\text{S}_{1-x}\text{Se}_x)_4$ and $\text{CuIn}(\text{S}_{1-x}\text{Se}_x)_2$ solid solution

XRD patterns presented in Fig. S4 demonstrate similar conclusion with $\text{Cu}_2\text{ZnSn}(\text{S}_{1-x}\text{Se}_x)_4$ samples. Fig. S4 (a) confirm the structure of $\text{Cu}_{2-y}(\text{S}_{1-x}\text{Se}_x)_4$ nanocrystals that prepared by the activated chalcogen precursor with different x values. The diffraction peaks are well indexed to planes (111), (200), (220), and (311), and the patterns can be assigned to bulk cubic Cu_{2-x}S (JCPDS No. 53-0522) and Cu_{2-x}Se (JCPDS No. 06-0680) respectively. A slight peak shift is observed as x value changes. As shown in Fig. S4 (b), the amplified diffraction peaks for (220) crystal plane show a decrease in 2θ values with increasing Se content. This is associated with the expansion of the lattice induced by increasing the content of Se, suggesting that S:Se ratios are tunable.

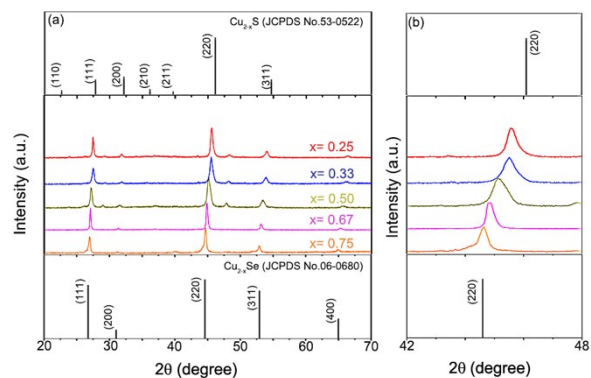


Fig. S4 XRD pattern for (a): Powder XRD patterns of $\text{Cu}_{2-y}(\text{S}_{1-x}\text{Se}_x)$ NCs samples with different x values that synthesized with the activated chalcogen precursor at 200 °C for 2 h. (b): Magnification of (220) crystal plane

Similar conclusion also got from $\text{CuIn}(\text{S}_{1-x}\text{Se}_x)_2$ samples. Fig. S5 (a) confirm the chalcopyrite structure of $\text{CuIn}(\text{S}_{1-x}\text{Se}_x)_2$ nanocrystals that prepared by the activated chalcogen precursor with different x values. The diffraction peaks are well indexed to planes (112), (200), (220), and (215), and the patterns can be assigned to CuInS_2 (JCPDS No. 38-0777) and CuInSe_2 (JCPDS No. 40-1487) respectively. A slight shift is observed in both XRD patterns as x value changes. As shown in Fig. S5 (b), the amplified diffraction peaks for (112) crystal plane show a decrease in 2θ values with increasing Se content.

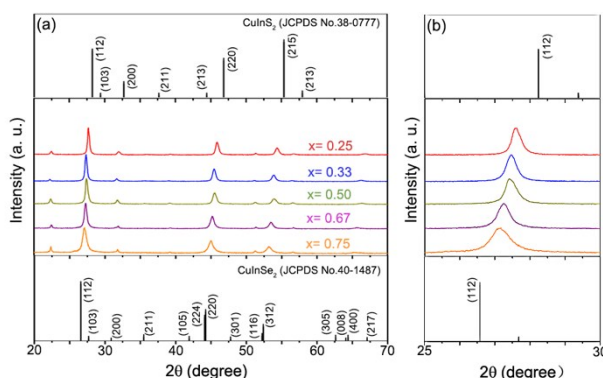


Fig. S5 XRD pattern for (a): Powder XRD patterns of $\text{CuIn}(\text{S}_{1-x}\text{Se}_x)_2$ NCs samples with different x values that synthesized with the activated chalcogen precursors at 200 °C for 2 h. (b): Magnification of (112) crystal plane

Table S3 and Table S4 confirm the composition of as-synthesized $\text{Cu}_{2-y}(\text{S}_{1-x}\text{Se}_x)$ NCs and $\text{CuIn}(\text{S}_{1-x}\text{Se}_x)_2$ NCs by EDS, illustrate that the element compositions in both samples are close to the stoichiometric chemical compositions and have roughly the same proportion of the raw materials.

Table S3 EDS analysis of the detailed composition and the proportional relation of as-prepared $\text{Cu}_{2-y}(\text{S}_{1-x}\text{Se}_x)$ samples with different x values

sample	Target product	Cu (at%)	S (at%)	Se (at%)	Cu/(S+Se)	Se/(S+Se)
1	$\text{Cu}_{2-x}(\text{S}_{0.75}\text{Se}_{0.25})_4$	67.35	23.85	8.79	2.06	0.27
2	$\text{Cu}_{2-x}(\text{S}_{0.67}\text{Se}_{0.33})_4$	66.69	22.94	10.37	2.00	0.31
3	$\text{Cu}_{2-x}(\text{S}_{0.5}\text{Se}_{0.5})_4$	65.91	16.51	17.58	1.93	0.52
4	$\text{Cu}_{2-x}(\text{S}_{0.33}\text{Se}_{0.67})_4$	64.99	11.28	23.73	1.86	0.68
5	$\text{Cu}_{2-x}(\text{S}_{0.25}\text{Se}_{0.75})_4$	64.61	8.73	26.67	1.83	0.75

Table S4 EDS analysis of the detailed composition and the proportional relation of as-prepared $\text{CuIn}(\text{S}_{1-x}\text{Se}_x)_2$ samples with different x values

sample	Target product	Cu (at%)	In (at%)	S (at%)	Se (at%)	Cu/(S+Se)	Se/(S+Se)
1	$\text{CuIn}(\text{S}_{0.75}\text{Se}_{0.25})_4$	27.41	27.14	32.68	12.09	1.01	0.27
2	$\text{CuIn}(\text{S}_{0.67}\text{Se}_{0.33})_4$	26.95	24.47	32.82	15.76	1.10	0.32
3	$\text{CuIn}(\text{S}_{0.5}\text{Se}_{0.5})_4$	27.14	24.41	23.28	25.17	1.11	0.52
4	$\text{CuIn}(\text{S}_{0.33}\text{Se}_{0.67})_4$	27.21	22.39	15.44	35.10	1.22	0.69
5	$\text{CuIn}(\text{S}_{0.25}\text{Se}_{0.75})_4$	25.63	22.97	12.37	39.02	1.12	0.76

Fig. S6 compares the value of $\text{Se}/(\text{S}+\text{Se})$ in $\text{Cu}_{2-y}(\text{S}_{1-x}\text{Se}_x)_2$ products and precursors. The values of $\text{Se}/(\text{S}+\text{Se})$ in products vary from 0.27 to 0.75 and are consistent with the S:Se ratios in precursors, indicating that the S:Se ratios can be simply tuned by changing the ratio of S and Se powder in precursors, which demonstrates that the reactivity of S and Se powders be not only improved but also balanced by NaBH_4 -activating. Additionally, the box chart in Fig. S3 exhibits the dispersion degree of the $\text{Se}/(\text{S}+\text{Se})$ in products determined by EDS, confirming that the presented time-saving solvothermal method is stable and repeatable

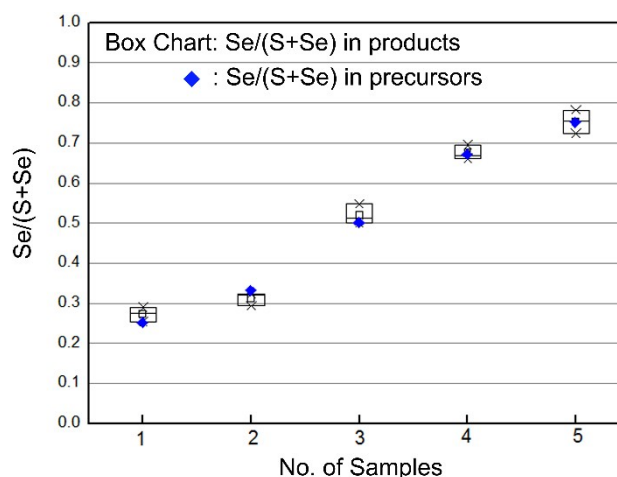


Fig. S6 Comparison of $\text{Se}/(\text{S}+\text{Se})$ between $\text{Cu}_{2-y}(\text{S}_{1-x}\text{Se}_x)_2$ products and precursors; Box chart exhibits the dispersion degree of $\text{Se}/(\text{S}+\text{Se})$ in products

Fig. S7 compares the value of $\text{Se}/(\text{S}+\text{Se})$ in $\text{CuIn}(\text{S}_{1-x}\text{Se}_x)_2$ products and precursors. The values of $\text{Se}/(\text{S}+\text{Se})$ in products vary from 0.27 to 0.76 and are consistent with the S:Se ratios in precursors, indicating that the S:Se ratios can be simply tuned by changing the ratio of S and Se powder in precursors, which demonstrates that the reactivity of S and Se powders be not only improved but also balanced by NaBH_4 -activating. Additionally, the box chart in Fig. S4 exhibits the dispersion degree of the $\text{Se}/(\text{S}+\text{Se})$ in products determined by EDS, confirming that the presented time-saving solvothermal method is stable and repeatable.

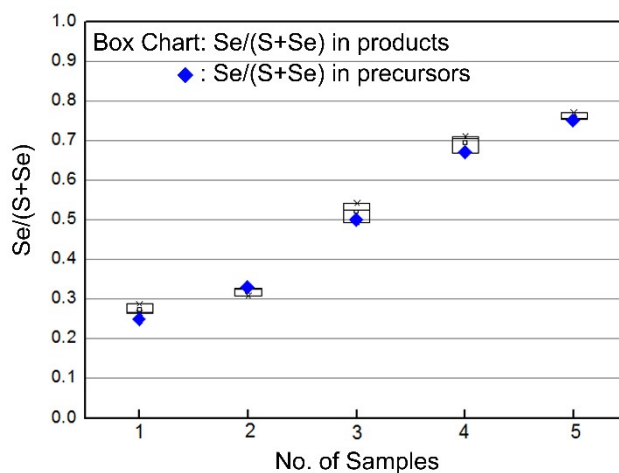


Fig. S7 Comparison of Se/(S+Se) between $\text{CuIn}(\text{S}_{1-x}\text{Se}_x)_2$ products and precursors; Box chart exhibits the dispersion degree of Se/(S+Se) in products

SEM images of $\text{Cu}_{2-y}(\text{S}_{1-x}\text{Se}_x)$ with different S:Se ratios are shown in Fig. S8. The synthesized particles possess a uniform morphology with an average size less than 100 nm. As the value of x increases, a small number of flake-shaped particles can be observed.

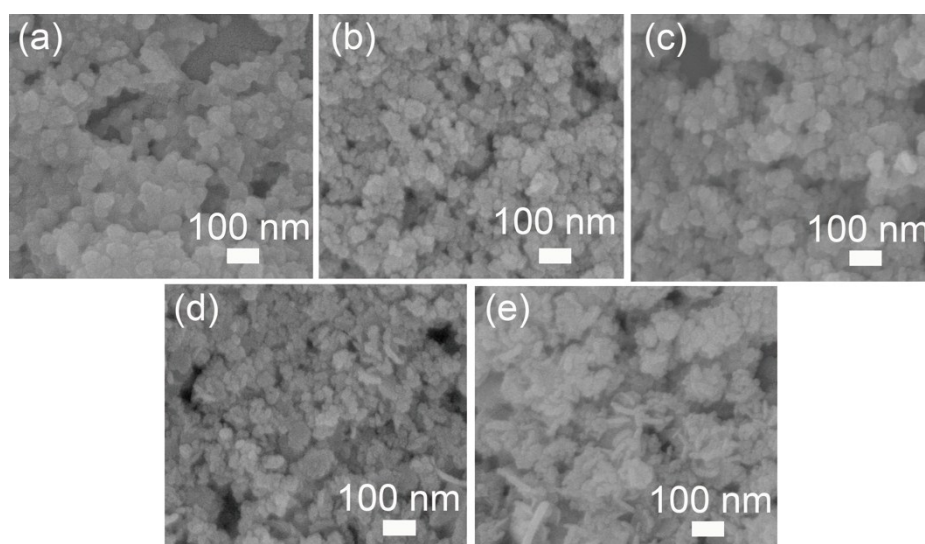


Fig. S8 SEM images of $\text{Cu}_{2-y}(\text{S}_{1-x}\text{Se}_x)$ NCs samples with different x values that synthesized with the activated chalcogen precursor at 200 °C for 2 h: (a) x=0.25; (b) x=0.33; (c) x=0.5; (d) x=0.67; (e) x=0.75.

SEM images of $\text{CuIn}(\text{S}_{1-x}\text{Se}_x)_2$ with different S:Se ratios are shown in Fig. S9. The products are flake-shaped nanoparticles. These nanoflakes further aggregate to form sub-micrometer-sized particles. As the value of x increases, the size of nanoflakes increases from ~100 nm to 1 μm .

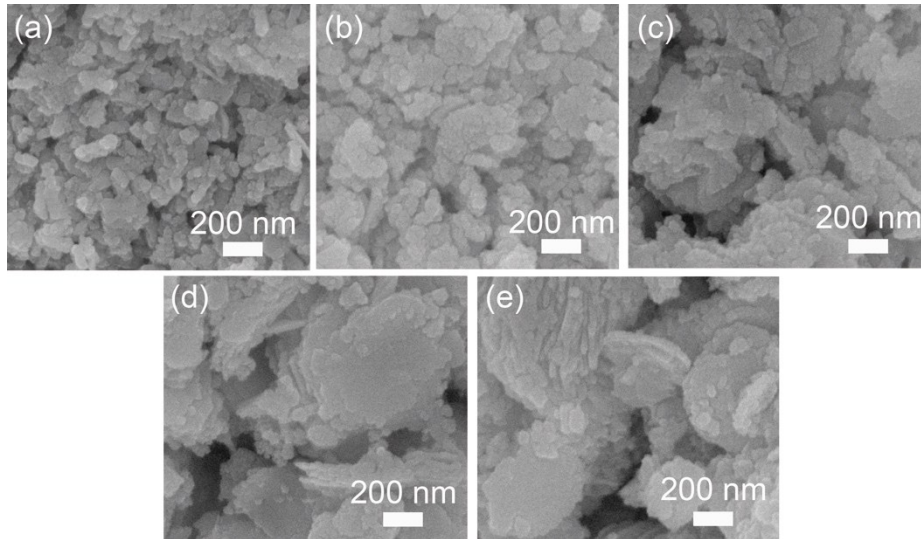


Fig. S9 SEM images of $\text{CuIn}(\text{S}_{1-x}\text{Se}_x)_2$ NCS samples with different x values that synthesized with the activated chalcogen precursors at 200 °C for 2 h: (a) $x=0.25$; (b) $x=0.33$; (c) $x=0.5$; (d) $x=0.67$; (e) $x=0.75$.

As shown in Fig. S10 (a) The E_g of $\text{Cu}_{2-x}(\text{S}_{1-x}\text{Se}_x)$ with different S:Se ratio ($x = 0.25, 0.33, 0.50, 0.67, 0.75$) are determined to be 1.47 eV, 1.41 eV, 1.27 eV, 1.21 eV, 1.13 eV, respectively. The E_g of $\text{Cu}_{2-y}(\text{S}_{1-x}\text{Se}_x)$ are plotted as a function of the Se/S+Se ratio in Fig. S10 (b), It can be noticed that the E_g of $\text{Cu}_{2-y}(\text{S}_{1-x}\text{Se}_x)$ increases monotonically with the decrease of the selenium content.

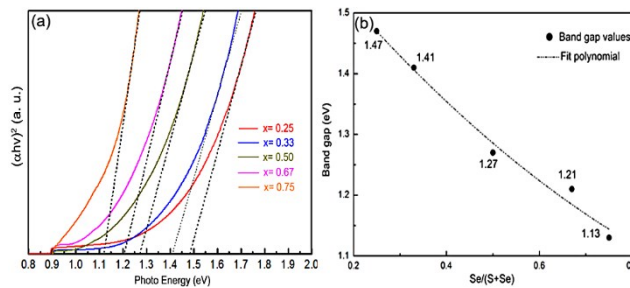


Fig. S10 (a) The band gap energy of $\text{Cu}_{2-y}(\text{S}_{1-x}\text{Se}_x)$ with different x values, (b) band gaps of $\text{Cu}_{2-y}(\text{S}_{1-x}\text{Se}_x)$ as a function of Se/S+Se.

As shown in Fig. S11 (a) The E_g of $\text{CuIn}(\text{S}_{1-x}\text{Se}_x)_2$ with different S:Se ratio ($x = 0.25, 0.33, 0.50, 0.67, 0.75$) are determined to be 1.31 eV, 1.25 eV, 1.17 eV, 1.12 eV, 1.08 eV, respectively. The E_g of $\text{CuIn}(\text{S}_{1-x}\text{Se}_x)_2$ are plotted as a function of the Se/S+Se ratio in Fig. S11 (b), It can be noticed that the E_g of $\text{CuIn}(\text{S}_{1-x}\text{Se}_x)_2$ increases monotonically with the decrease of the selenium content.

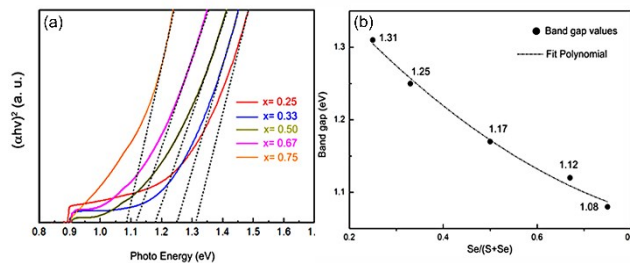


Fig. S11 (a) The band gap energy of $\text{CuIn}(\text{S}_{1-x}\text{Se}_x)_2$ with different x values, (b) band gaps of $\text{CuIn}(\text{S}_{1-x}\text{Se}_x)_2$ as a function of Se/S+Se